

Anomalous dynamics and the choice of Poincaré recurrence-set

Matteo Sala^{1,*}, Roberto Artuso^{2,3,†} and Cesar Manchein^{1‡}

¹*Departamento de Física, Universidade do Estado de Santa Catarina, 89219-710 Joinville, (Brazil)*

²*Center for Nonlinear and Complex Systems and Dipartimento di Scienza ed Alta Tecnologia, Via Valleggio 11, 22100 Como (Italy) and*

³*I.N.F.N., Sezione di Milano, Via Celoria 16, 20133 Milano (Italy)*

We investigate the dependence of Poincaré recurrence-times statistics on the choice of recurrence-set, by sampling the dynamics of two- and four-dimensional Hamiltonian maps. We derive a method that allows us to visualize the direct relation between the *shape* of a recurrence-set and the *values* of its return probability distribution in arbitrary phase-space dimensions. Such procedure, which is shown to be quite effective in the detection of tiny regions of regular motion, allows to explain *why* similar recurrence-sets have very different distributions and *how* to modify them in order to *enhance* their return probabilities. Applied on data, this permits to understand the co-existence of extremely long, *transient* power-like decays whose anomalous exponent *depends* on the chosen recurrence-set.

I. INTRODUCTION

One of the key issues in dynamical systems theory involves the analysis of stochastic features manifested by chaotic deterministic processes. In this regard a fundamental property is represented by the decay of temporal correlation functions: intuitively this is associated to loss of memory due to instabilities. We remind that correlation decay is associated to mixing, a stronger property than ergodicity in the hierarchy of chaotic indicators (see for instance [1]). When we focus on physical applications we are naturally led to better characterize the way in which correlations asymptotically vanish: while in the case of strongly chaotic systems an exponential decay is expected (and proved, in a very same way of space correlations for non critical lattice systems), the situation is considerably more complicated when a chaotic sea coexists with regular regions. In this case a typical chaotic trajectory gets trapped for very long time segments close to regular structures, significantly degrading the loss of memory in the dynamics. Such a “sticking” phenomenon [2–6] quantitatively leads to slow, polynomial decay of correlations (like in critical points of lattice models). A sharp characterization of the power law exponent is crucial on many respects: on the one side a sufficiently small exponent leads to the violation of the central limit theorem and might signal anomalous transport [3, 7] (since the diffusion constant in Green Kubo formula diverges when correlations are not integrable); on the other side, for important classes of Hamiltonian systems such exponents are conjectured to be universal [8, 9]. Direct calculation of correlation functions turns out to be a computationally demanding task, especially when, like in aforementioned cases, we need to span several decades in time in order to get clear indications of the appearance of power laws.

An alternative procedure, that introduces the main subject of the present paper, involves a statistical analysis of the *recurrence-times* of appropriate reference sets. The mathematical result that justifies such an approach is the Poincaré recurrence theorem [10], which states that *all* orbits of any volume-preserving transformation \mathbf{f} , acting on a *bounded* phase-space Ω of any finite dimension, eventually return arbitrarily near to their initial condition. More precisely, in any neighbourhood $U_{\mathbf{x}}$ of any point $\mathbf{x} \in \Omega$ there is a point \mathbf{y} that will come back to $\mathbf{f}^\tau(\mathbf{y}) \in U_{\mathbf{x}}$ in some unknown but *finite* time τ . Once we fix a reference set $B \subset \Omega$ we may thus investigate the *probability density* $\rho_B(\tau)$ of first recurrence-times (RT) through the fraction of initial conditions inside B that return to B , *for the first time*, exactly after τ iterations.

The relationship between such quantity and the general problems mentioned earlier lies in the fact that the product $\tau \cdot \rho_B(\tau)$ has the same asymptotic behaviour of correlation functions: this was early recognized [2, 11] in the analysis of ergodic properties of area-preserving mappings, and the correspondence has been mathematically proved [12, 13]. The effectiveness of this technique is witnessed by the large range of significant problems that have been addressed by RT statistics: from universal properties of Hamiltonian systems with mixed phase-space [8, 9, 14–17], to dynamical properties of comets in the solar system [18] and three-dimensional non-Hamiltonian models for fluid flows [19], to statistical properties of DNA molecules [20]. We point out that the most remarkable examples refer to polynomial decay of RT statistics (namely systems with long range memory): the transition from exponential to power-law decay of $\rho_B(\tau)$ has been extensively investigated for two-dimensional billiard tables [21].

Though the asymptotic behaviour of $\rho_B(\tau)$ at large RT’s is expected to be independent on the choice of recurrence-set B , arbitrarily long transients may be present, endowed with pre-asymptotic decay that may indeed depend upon the choice of B . These features

* matteo.sala.teo@gmail.com

† roberto.artuso@uninsubria.it

‡ cesar.manchein@udesc.br

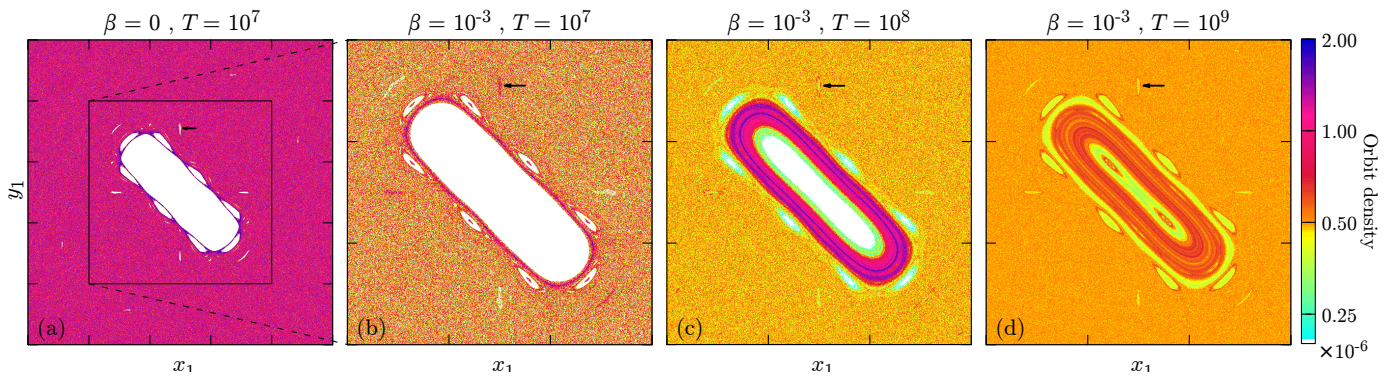


Figure 1. (Color online) Numerical orbit densities in the phase-space $(x_1, y_1) \in [0, 1]^2$ of map (1) with $K_1 = 0.65$, $K_2 = 0.60$. Panel (a) is the uncoupled case $\beta = 0$ (single standard-map) after $T = 10^7$ iterations; panels (b), (c) and (d) are magnifications of the square $[0.2, 0.8]^2$ (depicted in panel (a)) for $\beta = 10^{-3}$ respectively after $T = 10^7$, 10^8 and 10^9 iterations. While the standard-map density exhibits *accumulations* (panel (a), purple/dark-gray cells) at the borders of stability-islands (white color indicates unvisited cells), the latter become accessible to the coupled map, although at extremely slow rates: at equal times (panel (b)), the system just started to penetrate areas *forbidden* to the standard-map. Only at much longer times $\sim 10^9$ (panel (d)), phase-space exploration appears complete but anisotropies are still present. Such *filling* time-scale diverges in the limit of vanishing coupling $\beta \rightarrow 0$, while there is a *threshold* $\beta_* < \beta$ above which map (1) is completely ergodic [26, 27] (see Sec. IV C).

are of particular relevance in the investigation of Hamiltonian systems with mixed phase-space, where, after a *transient*, the decay of *integrated* RT probabilities $P_B(\tau) = \sum_{t \geq \tau} \rho_B(t) \sim \tau^{-\gamma}$ turns algebraic. While the asymptotic exponent γ is assumed to be independent on B (and, for 2D Hamiltonian maps, there are arguments supporting its universality $\gamma_{2D} \simeq 1.6$ [8, 14, 15, 22]), no general statements are known about the transient behaviour and its length (precise results on the full probability distribution are only available in the limit of increasingly small recurrence-sets B , see [23] and references therein). When we increase the dimensionality $N > 2$ there are a few numerical investigations (for small and moderate numbers of *homogeneously* coupled 2D maps) that again suggest a (universal) asymptotic exponent $\gamma_{ND} \simeq 1.2$ [9, 16, 20], but it is still under debate whether such value persists in the weak-coupling regime. In particular, it remains unclear how to estimate the *time-scale* over which a higher-dimensional system reaches its asymptotic regime under the process of *weak* Arnol'd diffusion [24, 25]. In this work we address such problem by linking the *diffusive strength* along a specific coupling-transition across its *ergodic threshold* (see [26, 27] and references therein) to the *dependence* of RT's on the choice of recurrence-set B .

The paper is organized as follows: while in Sec. II we introduce the four-dimensional model under study, in Sec. III we describe how recurrence data is generated and collected by our numerical experiments, providing the due mathematical background through appendices. On such grounds, in Sec. IV we present our numerical results: by the developed methods we have access to an efficient *detector* for all phase-space structures that are responsible for *long* recurrences (down to very small scales, see Sec. IV A) which, in turn, suggests a recipe

to systematically *enhance* RT probabilities by changing a specific *universal* property of the chosen set (namely, the *size* of its *departure-set*, see Sec. IV B). By performing our novel RT analysis to several recurrence-sets B in comparing different parameters for system II, in Sec. IV C we confirm the existence of extremely long sub-diffusive transients with pre-asymptotic exponent γ_B *dependent* on set B . After exploiting the aforementioned detector to also *identify* the phase-space structures responsible for such a non-trivial dependence, in Sec. V we summarize our results indicating some of their possible implications.

II. MODEL

We consider as benchmark system a pair of coupled 2D Chirikov-Taylor standard-maps [28], defined on the unit torus $(x_j, y_j) \in [0, 1]^2 = \mathbb{T}^2$ for $j = 1, 2$ and evolving by:

$$\begin{cases} \bar{x}_j = 2x_j - y_j + f_j(x_1, x_2) \pmod{1}, \\ \bar{y}_j = x_j, \end{cases} \quad (1)$$

with both local (K_j) and coupling (β) *conservative* non-linear forces which, setting $\delta x = x_1 - x_2$, are given by:

$$f_j(x_1, x_2) = K_j \sin(2\pi x_j) + \beta (-1)^j \sin(2\pi \delta x). \quad (2)$$

Map (1) is four-dimensional *symplectic* (phase-space is $\Omega = [0, 1]^4 = \mathbb{T}^4$), with single 2D standard-maps written in McMillan form [29] to fully exploit their symmetry structure (see the orbit densities in Fig. 1). Indeed, in such coordinate system, each 2D standard-map (x, y) in (1) at $\beta = 0$ maps vertical lines $x = x_0$ into their symmetric horizontal lines $y = x_0$ *independently* from the specific local force $K \sin(2\pi x)$, which only sets a *shift* along the reflected line itself. Interestingly, all vertical lines inside the rectangular set B sketched in

Fig. 2 (bordered by pink/gray dashed line) are thus reflected, but also non-linearly shifted along themselves and wrapped over the torus; as a consequence, set B is transformed into $B_1 = \mathbf{f}(B)$ (bordered by blue/black dash-dotted line) whose *shape* coincides with B reflected about the bisector.

Although in different coordinates, the same system is studied in [27] for several numbers of *identical* coupled maps $K_j = K, \forall j$, confirming the existence of a coupling *threshold* $\beta > \beta_*$ above which dynamics appears ergodic. A similar interaction force $\pm\beta \sin(2\pi(x_1 + x_2))$ is also considered in [30], finding a non-trivial structure of *resonances* between the two 2D standard-maps. Local forces $K \sin(2\pi x)$ ensure that system (1) is chaotic also when it is uncoupled, at $\beta = 0$. To get a generic case, we fix the parameters $K_1 = 0.65$ and $K_2 = 0.60$ [37], both corresponding to well-developed chaotic regimes with strongly *mixed* phase-spaces, due to the co-existence of a main hyperbolic fixed-point at $(x, y) = (0, 0)$ with a central system at $(x, y) = (0.5, 0.5)$. While for $K_2 = 0.60$ the latter is a stable fixed-point with a typical surrounding hierarchy of un/stable tori, for $K_1 = 0.65$ it is made by a *weakly* hyperbolic fixed-point with *eight-shaped* homoclinic intersections encircling a *stable* orbit of period 2. Remarkably, in the uncoupled regime (Fig. 1 (a), $\beta = 0$) the central system is *completely* isolated from the main chaotic sea by a thick, quasi-periodic annular barrier. Once the coupling is on (Fig. 1 (b)-(d) for $\beta = 10^{-3}$), the orbits are allowed to penetrate the barrier and access the central system, although at gradually slower rates as $\beta \rightarrow 0$, *de facto* inducing the process of *weak* Arnol'd diffusion. Operatively, by the coupling parameter-range $10^{-6} \leq \beta \leq 10^{-3}$ we observe weakly *correlated* kicks, given by $\pm\beta \sin(2\pi \delta x)$, driving each of the two maps in and out what become *broken* tori. The latter appear to be alternatively selected/avoided by the orbits in a very complicated way, which sensibly depends on the initial condition: an example is shown in Fig. 1 (b)-(d) by a single orbit that accumulates more over *just* one of two *symmetric* period-3 island-chains with very thin shape (the arrow points to one of the three selected islands). By changing initial condition (not shown) it is possible to revert such *sticky* behaviour to the other period-3 island-chain, or even to *avoid* it, highlighting the existence of markedly *separate* paths by which orbits can penetrate and diffuse inside the broken central system.

III. DATA COLLECTION

The standard procedure to collect a single event τ in the RT statistics involves what is called a *Poincaré cycle* [31]. In spite of being a very old recipe, this deserves to be examined with care, more than for clarity, for the useful information it encodes. Informally, indeed, one can describe the procedure as: measure the lapses of time spent outside set B by an orbit started in

B . Here we focus on the single recurrence cycle and, by referring to Fig. 2, picture it as follows: an orbit starts from point \mathbf{x} in set B (bordered by pink/gray dashed line) and evolves as long as it remains *inside* B (solid bullets). The *residence period* inside set RES_B (dark-red/dark-gray zone) lasts until landing in what we call the *departure-set* D_B (green/gray zone), made by all points \mathbf{x}_1 that escape from B in *one* iteration into $B_1 = \mathbf{f}(B)$ (bordered in blue/black dash-dotted line). Notice that this new set is constructed by $D_B = B_1 \setminus B$, *i.e.* by subtracting from set B_1 all points that are still in B . From such first point $\mathbf{x}_1 \in D_B$ lying outside B , we start a clock $t_B(\mathbf{x}_1) = 1$ and employ it to label all successive iterates $\mathbf{x}_t \notin B$ that stay outside B , in REC_B (white zone) by setting $t_B(\mathbf{x}_t) = t$ (red/empty circles). A cycle ends once the orbit returns to B after a number $t = \tau$ of clock ticks, which marks its Poincaré RT (length). By repeating the substitution $\mathbf{x} \leftarrow \mathbf{x}_{\tau+1} \in B$ a number E of times, we thus collect RT statistics over an ensemble made of E Poincaré cycles (events) sampled from a single trajectory started in B (see Appendix A).

All points $\mathbf{x}_{\tau+1}$ hitting B first belong to what we call the *arrival-set* A_B (yellow/light-gray zone in Fig. 2) which is the *only* set accessible from outside B in one step. Notably, the arrival-set has a general expression $A_B = B \setminus B_1$ which is similar to the departure-set

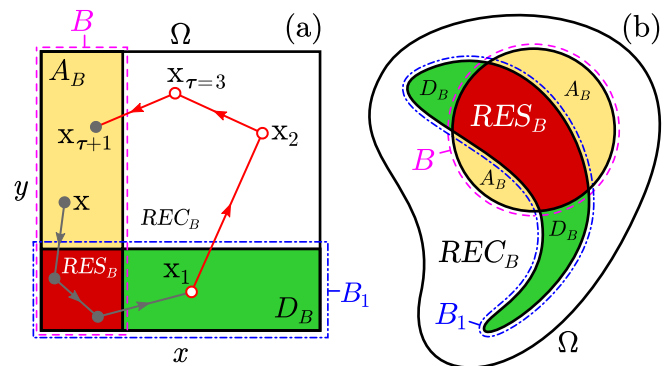


Figure 2. (Color online) Panel (a): scheme of a single Poincaré cycle as described in Sec. III for one uncoupled ($\beta = 0$) standard-map in (1) and recurrence-set B (bordered by pink/gray dashed line) in the phase-space $\Omega = [0, 1]^2$ (largest square), with departure-set $D_B = B_1 \setminus B$ (green/gray zone) and arrival-set $A_B = B \setminus B_1$ (yellow/light-gray zone); recurrence/residence cycles take place only in the respective sets REC_B/RES_B . In these coordinates, first iterated-set $B_1 = \mathbf{f}(B)$ (bordered by blue/black dash-dotted line) has the same shape of B reflected about the bisector. Panel (b): picture of the four sets D_B, REC_B, A_B and RES_B as described in Appendix B for a dynamics $B \rightarrow B_1 = \mathbf{f}(B)$ induced by evolving a generic flow $\mathbf{f} = \mathcal{F}^{\Delta t}$ along a fixed time-step Δt ; standard-map in panel (a) belongs to the special class of *time-periodic* Hamiltonian flows whose integration after one period Δt admits an *explicit* expression, as the one used in equation (1).

$D_B = B_1 \setminus B$ and shares with it the same volume $\mu(A_B) = \mu(D_B)$. By fixing set B , any bounded phase-space Ω is then partitioned into four sub-sets D_B , REC_B , A_B and RES_B respectively associated to the *universal* processes of: departure, recurrence, arrival and *residence* in B (in Fig. 2, green/gray, white, yellow/light-gray and dark-red/dark-gray zones), whose shape is induced by both the dynamics and the recurrence-set B . This suggests that the departure/arrival-sets D_B and A_B are the *unique* channels between escape and return cycles, which practically means that the departing volume $\mu(D_B) = \mu(A_B)$ measures the *rate* per single iteration at which a volume-preserving dynamics extracts/re-injects orbits from a set B (see Appendix B).

Such mechanism is better understood by inspection of the employed clock $t_B(\mathbf{x})$, which we name *Poincaré-time* (PT): this is the time $t_B(\mathbf{x})$, since *last* exit, spent by a Poincaré cycle to reach point $\mathbf{x} \in \Omega \setminus B$ lying *outside* B . In case \mathbf{f} is a mapping, PT is an integer-valued *function* which ranges from 1 to τ when observed over a cycle of length (RT) equal τ . Consequently, once PT is evaluated over ensembles of cycles (*i.e.* volumes outside B), the PT level-sets S_B^τ , made of points \mathbf{x} with *constant* PT value:

$$S_B^\tau := \{ \mathbf{x} \in \Omega \setminus B \text{ s.t. } t_B(\mathbf{x}) = \tau \}, \quad (3)$$

reveal the shapes of all the higher iterates $B_\tau = \mathbf{f}^\tau(B)$ of set B . Indeed, in Appendix C we show how the whole set-family $\{S_B^\tau\}_{\tau=1,2,\dots}$ can be generated by the universal recursive relation $S_B^{\tau+1} = \mathbf{f}(S_B^\tau) \setminus B$ with departure-set $S_B^1 = B_1 \setminus B = D_B$ as initial condition at PT $\tau = 1$. In conjunction with Appendix D, we also prove that all the volumes $\mu(S_B^\tau)$ of the PT level-sets family can be used to express the full RT probability $P_B(\tau) = \text{Prob}(\text{RT} \geq \tau)$:

$$P_B(\tau) = \mu(S_B^\tau) / \mu(D_B). \quad (4)$$

by *normalizing* them exactly by the departing volume $\mu(D_B)$, as suggested by our preliminary considerations. Novel expression (4) highlights a fundamental fact: RT probabilities decay *exactly* as the PT level-sets volumes $\mu(S_B^\tau) \rightarrow 0$, *weighted* by the departing volume $\mu(D_B)$. While the latter acts as a pre-factor to the asymptotic decay (which is assumed to be independent on set B), formula (4) already shows that *transient* RT statistics is entirely implied by the *relative* size of PT level-sets S_B^τ for $\tau = 2, 3, 4, \dots$ with respect to the first departure-set $S_B^1 \equiv D_B$. Such universal property is the key ingredient upon which we base our analysis of the dependence of RT statistics on the choice of recurrence-set.

IV. RESULTS

The considerations from previous section III (see also the Appendices for more detailed discussions) find their application in two fundamental aspects of the same problem: RT probabilities $P_B(\tau)$ depend on both the *intrinsic*

structure of phase-space (induced by dynamics) and the *external* choice of recurrence-set (chosen by observers). Poincaré-time functions (PT) provide a rigorous method to *chart* and identify all the *localized* sources of long RT's, for all the conservative systems in higher-dimensions. By employing PT as a *detector* for extremely small phase-space structures (see Sec. IV A), we also find a simple recipe which allows to *shift* in τ the RT probability $P_B(\tau)$ by appropriately changing the *shape* of recurrence-set B (see section IV B). Finally, by combining such findings, we are able to assess a *lower-bound* for the transient time-scale of RT statistics (see section IV C) for the four-dimensional system presented in Eq. (1).

A. Phase-space structures detection

In figure 3, we start by applying expression (4) for RT statistics to the single standard-map $K = 0.65$, which corresponds to the uncoupled regime of four-dimensional map (1) at $\beta = 0$. In panel (a), the unit-square

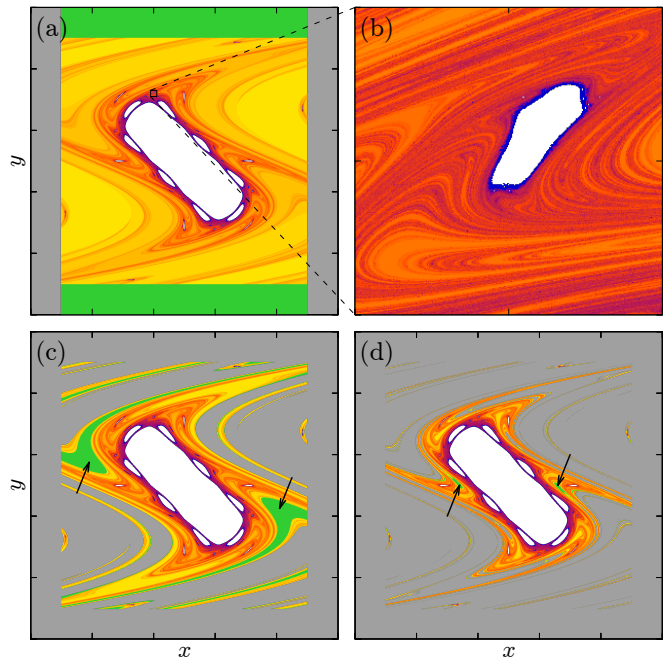


Figure 3. (Color online) Panel (a): Poincaré-time (PT) function for the same uncoupled standard-map as in Fig. 1 (a) with recurrence-set $B_{[0.1]} = \{|x_1| < 0.1\}$ (gray rectangles), departure-set D_B (green/dark-gray rectangles) and PT level-sets S_B^τ as in Eq. (D2) with colors encoded by the τ axis in Fig. 4; white color indicates cells *unvisited* by Poincaré cycles. Panel (b): magnification of the square $[0.39, 0.41] \times [0.71, 0.73]$ from panel (a), detecting islands structures of extremely small area $\sim 10^{-8}$. Panels (c) and (d): same PT analysis as panel (a) for two *lag-sets* $I_B^{\delta\tau}$ as in Eq. (5) (gray cells) respectively for $\delta\tau = 5$ and 10. The lag-sets departing volume $\mu(D_{I_B^{\delta\tau}})$ (green/dark-gray cells indicated by arrows) *shrinks* as we rise $\delta\tau$.

phase-space $(x, y) \in [0, 1]^2$ contains the recurrence-set $B_{[0.1]} = \{|x| < 0.1\}$ (gray rectangles) and its departure-set $D_B = B_1 \setminus B$ (green/dark-gray rectangles) as discussed in Sec. III and defined in Appendix B. The PT level-sets $S_{[0.1]}^\tau \equiv S_{B_{[0.1]}}^\tau$ for higher values of τ are approximated [36] by the \mathcal{G} -averaged PT function $\langle t_B \rangle_{\mathcal{G}}$ computed over a square-grid \mathcal{G} with $10^3 \times 10^3$ cells by the recipe described in Appendix C. As explained there, the PT probability-density *coincides* with the RT probability, so that each color in Fig. 3 encodes a PT value which corresponds to the color-scale along the τ axis in Fig. 4 while the value of $P_B(\tau)$ can be also interpreted as the *fraction* of cells with such color (PT value) among grid \mathcal{G} .

At once, this allows to chart and visualize the natural partition of phase-space induced by the association of each PT level-set (color) to a specific time-scale in the RT statistics: range $\tau < 10^2$ (colors from yellow/light-gray to dark-orange/gray) is associated to the chaotic-sea generated by the main unstable fixed-point at $(x, y) = (0, 0)$ while the ranges $10^2 \leq \tau < 10^3$ (from dark-orange/gray to dark-magenta/dark-gray) and $10^3 \leq \tau < 10^4$ (from dark-magenta/dark-gray to blue) appear to be generated by sub-diffusion respectively through a *symmetric pair* of very thin period-3 island-chains (one of which is indicated by arrows in Fig. 1) and the barrier made by a single period-8 island-chain. The highest recorded values of $\tau \sim 10^4$ (bins in blue color in Fig. 4) are associated to the *sticky motion* around the main stable-island and are located in the distribution tail, exactly where RT probabilities $P_B(\tau) \sim 10^{-6}$ approach the cell-area of grid \mathcal{G} ; the latter is thus *insufficient* to resolve the phase-space details of higher PT level-sets.

Indeed, by fixing a time-scale $\tau > \tau^*$ one gets a *unique* probability-threshold $P_B(\tau) < P_B^*$ which, by Eq. (4), automatically implies an *upper-bound* for each level-set volume $\mu(S_B^\tau) < \mu(S_B^1) \times P_B^*$. This makes the cell-averaged PT function $\langle t_B \rangle_{\mathcal{G}}$ a fast *presence detector* for phase-space regions responsible for very long RT's (such as micro-islands in strongly chaotic backgrounds) based on the *time-scale* τ at which each of such structures contributes to the RT statistics. A direct example of these considerations is shown in Fig. 3 (b) by a magnification of panel (a) by a grid \mathcal{G}' with 300×300 cells over the square $(x, y) \in [0.39, 0.41] \times [0.71, 0.73]$: the higher iterates B_t of set B naturally tend to align to the unstable manifolds as $t \rightarrow \infty$ [38], providing their structure in the neighbourhood of resonances *while* localizing smaller islands, possibly for further magnifications. Notice that this method outperforms existing detectors both in the observable scales *and* computational cost [32, 39].

B. RT Probability enhancement

Among their possible applications in data analysis [40], PT functions allow to perform a direct comparison

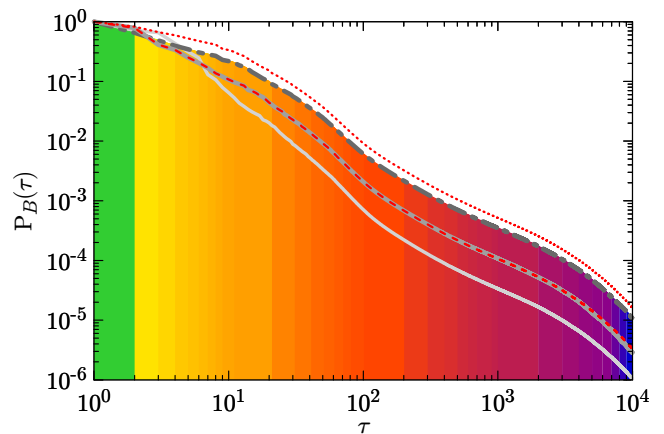


Figure 4. (Color online) RT probability (light-gray continuous curve) for the recurrence-set B in Fig. 3, panel (a) and its *lag-sets* $I_B^{\delta\tau}$ with lags $\delta\tau = 5$ (dashed red/black curve, set in Fig. 3 (c)) and $\delta\tau = 10$ (dotted red/black curve, set in Fig. 3 (d)) as in Eq. (6). The predicted probabilities for $I^{\delta\tau}(B)$ are matched in the case $\delta\tau = 5$ (continuous gray curve for the set $I^5(B_{[0.1]})$ in Fig. 3 (c)) while they are underestimated in the case $\delta\tau = 10$ (dash-dotted dark-gray curve for the set $I^{10}(B_{[0.1]})$ in Fig. 3 (d)). Despite this, both cases produce RT probability *enhancement*.

between the different *sizes* of localized RT sources. In particular, from Sec. III and Appendix C we know that the departing volume $\mu(D_B)$ fixes the *maximal* size $\mu(D_B) \geq \mu(S_B^\tau)$ of all the PT level-sets S_B^τ generating the RT statistics $P_B(\tau)$, whose decay is completely determined by the *relative* size between sets S_B^τ and $S_B^1 \equiv D_B$. If the latter is much *larger* than the formers, at short recurrences τ_* the RT probability $P_B(\tau < \tau_*)$ *falls* abruptly. Conversely, by opting for recurrence-sets B whose departing volume $\mu(D_B) \ll 1$ is sufficiently small to have the first τ_* level-sets volumes $\mu(S_B^{\tau < \tau_*}) \simeq \mu(S_B^1)$ *comparable*, we get an automatic *raise* of the first τ_* RT probabilities. This is a consequence of the fact that small departing volumes $\mu(D_B) = \mu(B_1 \setminus B) \simeq 0$ imply to have $B \simeq \mathbf{f}(B)$, that is, recurrence-sets that are *almost-invariant*. In fact, the limit case of *invariant-sets* $B = B_1$ saturates to 1 all RT probabilities: $P_B(\tau) = 1$ for all τ and B .

Inspired by such ideas and to avoid expensive procedures to find and test new sets which are *also* almost-invariant, we define a family of sets as *automatic* extensions of any, possibly already tested, set B . These sets are made by *joining* to set B all its iterates $B_{t=1,2,\dots,\delta\tau}$ until some *lag-time* $\delta\tau$. Accordingly, we name these the $\delta\tau$ -th *lag-sets* $I^{\delta\tau}(B)$ acting over an arbitrary set B :

$$I^{\delta\tau}(B) = \bigcup_{t=0}^{\tau} B_t. \quad (5)$$

This construction is strongly motivated by the fact that each new PT level-set $S_{I^{\delta\tau}(B)}^\tau = S_B^{\tau+\delta\tau}$ for set $I^{\delta\tau}(B)$ is

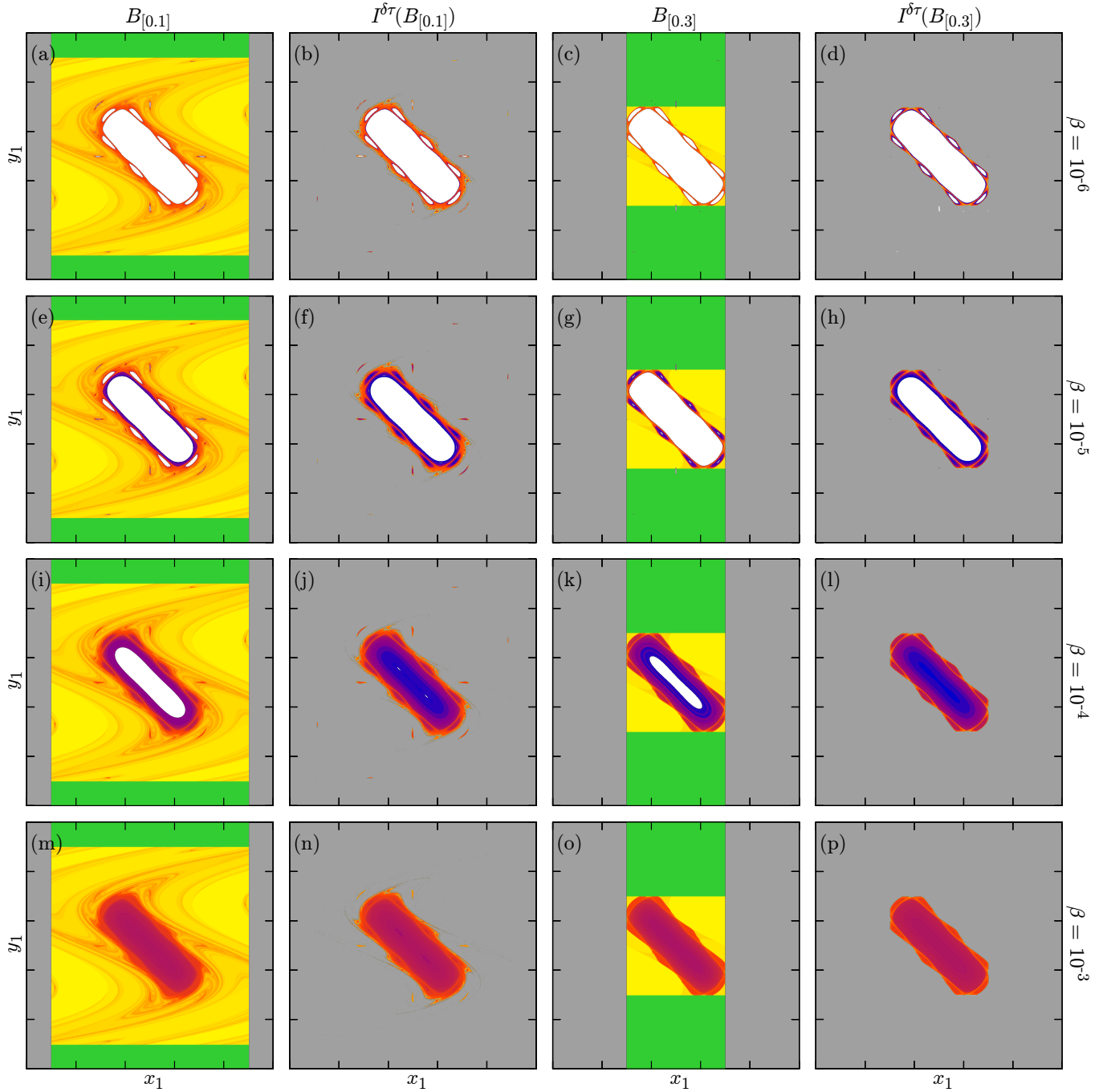


Figure 5. (Color online) Same Poincaré time (PT) function analysis as in Fig. 3 in phase-space $(x_1, y_1) = [0, 1]^2$ for the first of the two maps in Eq. (1) at four coupling regimes: $\beta = 10^{-6}$, 10^{-5} , 10^{-4} and 10^{-3} (respectively from first to fourth row) for the recurrence-sets $B_{[0.1]} = \{|x_1| < 0.1\}$ and $B_{[0.3]}$ and their lag-sets $I^{\delta\tau}(B_{[0.1]})$ and $I^{\delta\tau}(B_{[0.3]})$ (gray zones, respectively from first to fourth column) with lag-time $\delta\tau = 200$ in Eq. (5). Colors are encoded by the τ axis in Fig. 6, as $\mu(S_B^{\tau}) \propto P_B(\tau)$ by Eq. (4), with green/dark-gray color for D_B (for lag-sets $I^{\delta\tau}$, the latter is made of a few cells) and white color for unvisited cells.

exactly the old $(\tau + \delta\tau)$ -th PT level-set for set B , which implies a straightforward relation between the *old* $P_B(\tau)$

and the *new* $P_{I^{\delta\tau}(B)}(\tau)$ RT probability:

$$\begin{aligned} P_{I^{\delta\tau}(B)}(\tau) &= \mu(S_B^{\tau+\delta\tau}) / \mu(S_B^{1+\delta\tau}) \\ &= P_B(\tau + \delta\tau) / P_B(1 + \delta\tau). \end{aligned} \quad (6)$$

This is akin to say that the *lagging* of a recurrence-set

$B \rightarrow I^{\delta\tau}(B)$ shifts by $\delta\tau$ its RT statistics while scaling it by $P_B(1 + \delta\tau)$. In Fig. 3 we apply such recipe for two values of lag-time $\delta\tau = 5$ and 10 (respectively panel (c) and (d), white cells), by “turning white” all cells in panel (a) that, for rectangular set $B_{[0,1]}$, have \mathcal{G} -averaged PT function $\langle t_{B_{[0,1]}} \rangle_{\mathcal{G}} \leq \delta\tau$ below the respective lag-time $\delta\tau$. While any lag-set $I^{\delta\tau}(B)$ is always bigger than B (otherwise no point would ever exit from B), we confirm that the corresponding departing volume is smaller and it shrinks for longer lags (see arrows in Fig. 3 (c) and (d)), since the PT level-set volumes $\mu(S_B^{\delta\tau+1}) \rightarrow 0$ are monotonic decreasing in the lag-time $\delta\tau \rightarrow \infty$. Alongside, in Fig. 3 (d) we also notice very filamentary structures in the shape of set $I^{10}(B_{[0,1]})$, with details having size below the cell-area scale. Unsurprisingly, the corresponding RT probabilities shown in Fig. 4 reveal that only the first case matches the theory ($\delta\tau = 5$, continuous gray curve vs Eq. (6), dashed red/dark-gray curve) while the second case ($\delta\tau = 10$, dash-dotted gray curve) underestimates prediction (6) (dotted red/dark-gray curve) because of the finite-size of our lag-sets approximation. By the latter, we are thus able to control the departing volume $\mu(D_{I_B^{\delta\tau'}}) \leq \mu(D_{I_B^{\delta\tau}})$ and progressively enhance the RT probabilities by employing larger lag-times $\delta\tau' > \delta\tau$, but there is a maximal effective lag $\delta\tau_*$ which limits the observations that are made at fixed resolution of square-grid \mathcal{G} . Remarkably, indeed, the formal infinite-lag limit $\delta\tau \rightarrow \infty$ for Eq. (6), saturates to 1 the RT probability $P_{I^{\delta\tau}(B)}(\tau) \rightarrow 1$ for all τ and sets B , so that I_B^∞ is the invariant-set covering the whole volume that is accessible from the chosen set B .

C. Weak-chaos transition

Once testing the lag-set recipe described in Sec. IV B on the four-dimensional map (1) for $\beta > 0$ we must take into account that, in addition to the coarse-grain induced by square-grid \mathcal{G} , the lag-sets are approximated through the relation: $I^{\delta\tau}(B) \simeq \{\langle t_B \rangle_{\mathcal{G}} \leq \delta\tau\}$, with the \mathcal{G} -averaged time-of-flight $\langle t_B \rangle_{\mathcal{G}}$ being the projection on a single map 2D phase-space (x_1, y_1) of the true four-dimensional PT function $t_B(x_1, x_2, y_1, y_2)$. Such estimate, which involves only the shape of our lag-sets once we need to numerically employ them as recurrence-sets (the dynamics of map (1) at $\beta \neq 0$ is fully 4D), is acceptable in the weak-coupling regime, since the uncoupled case $\beta = 0$ has PT function $t_B(x_1, y_1)$ in 2D exactly. In fact, we expect this approximation to be effective even over very long time-scales, since the main point here is about the reduction of departing volume $\mu(D_B)$, regardless the computational issue of approximating increasingly complex recurrence-sets.

Such reasoning is supported by the numerical application of the lagging procedure $B_{[0,1]} \rightarrow I^{\delta\tau}(B_{[0,1]})$ for $\delta\tau = 200$ (in Fig. 5, first column of panels is $B_{[0,1]}$, sec-

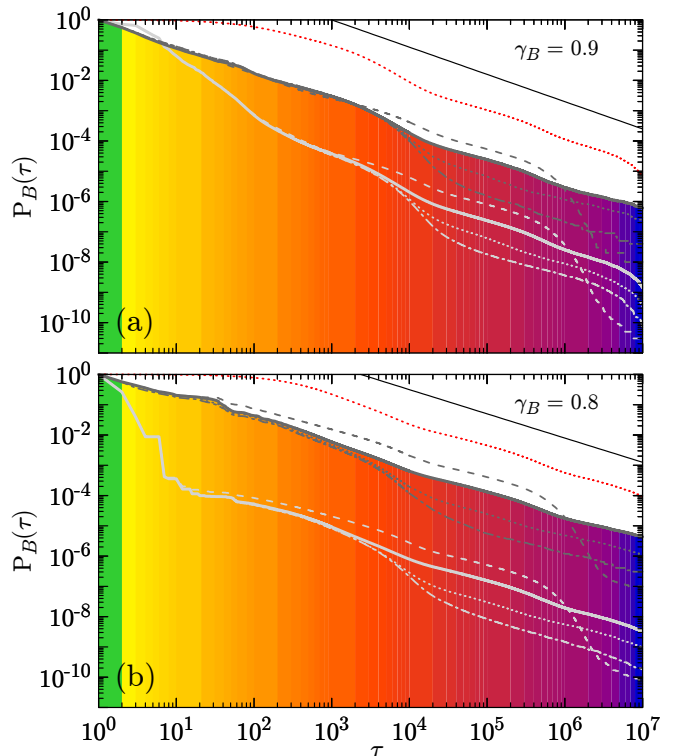


Figure 6. (Color online) RT probability for recurrence-sets $B_{[0,1]}$ and $B_{[0,3]}$ (gray curves respectively in panel (a), (b)) pictured in Fig. 3 respectively in first and third column. The line-types correspond to $\beta = 10^{-3}$ (dashed), 10^{-4} (continuous), 10^{-5} (dotted) and 10^{-6} (dash-dotted). The two families of gray curves correspond to $I^{\delta\tau}(B_{[0,1]})$ (panel (a)) and $I^{\delta\tau}(B_{[0,3]})$ (panel (b)) with lag $\delta\tau = 200$ and pictured in Fig. 3 respectively in second and fourth column. Thin red/dark-gray dotted curves in both panels are the light-gray continuous ones ($\beta = 10^{-4}$) shifted by $\delta\tau$ as in Eq. (6) for the exact lag-sets.

ond column is $I^{200}(B_{[0,1]})$): by drastically reducing the departure-set to few grid-cells, in Fig. 6 (a) we get the corresponding RT probabilities enhanced by ~ 2 orders of magnitude, but also underestimate formula (6) by a similar factor (compare black curves for lag-set $I^{200}(B_{[0,1]})$ with the gray ones for the original $B_{[0,1]}$ and the dotted red/dark-gray curve for its theoretical shift by $\delta\tau = 200$ as given by Eq. (6)). In agreement with the previous case at $\beta = 0$ and $\delta\tau = 10$ in Fig. 3 (d), our fixed square-grid \mathcal{G} is again insufficient in resolving the lag-set details for such a large lag $\delta\tau = 200$, since the filamentation scale is now of order $\sim e^{-200\Lambda}$ with Λ the maximal Lyapunov exponent of the system.

These observations lead to a first important conclusion: RT probabilities can be enhanced by reducing the size of departure-set to some minimal computable area (in our case, few grid-cells) even if the chosen recurrence-set is not the exact lag-set of some other set. This makes the departing volume $\mu(D_B)$ a robust and thus useful parameter in the choice of any recurrence-set.

Interestingly, by inspection of second column in Fig. 5 for $I^{\delta\tau}(B_{[0.1]})$, one can notice that the pair of period-3 island-chains (see the arrows in Fig. 1) is not removed by the lagging procedure, because the return time-scale of such resonances is longer than the chosen lag $\delta\tau = 200$. Indeed, in Fig. 1 (c) for $\beta = 10^{-3}$, such particular island-chains still show persistent effects on orbit densities at times $\tau \sim 10^8$ larger than the maximal observed RT = 10^7 , denoting very strong stickiness. In order to test which is the effect of such period-3 structures on the RT statistics, in Fig. 5 we *forcibly exclude* them from the latter by taking a larger rectangular set $B_{[0.3]} = \{|x_1| < 0.3\}$ and its corresponding lag-set $I^{\delta\tau}(B_{[0.3]})$, again for a lag-time $\delta\tau = 200$ (third column is $B_{[0.3]}$, fourth column is $I^{200}(B_{[0.3]})$). Set $B_{[0.3]}$ is chosen to overlap the targeted period-3 island-chains and *transfer* their dynamical contribution to its *residence-times* statistics [41]. Such property is preserved by all lag-sets $I^{\delta\tau}(B_{[0.3]})$ so that, in Fig. 6(b) (light-gray curves for $B_{[0.3]}$ and gray curves for $I^{200}(B_{[0.3]})$) we observe the *same* ergodic transition from panel (a), but now *without* the RT contribution of the period-3 structures. Quite interestingly, the comparison between panels (a) and (b) in Fig. 6 (both gray and light-gray curves) highlights two different power-law decays with appreciably different exponents $\gamma_{[0.1]} \simeq 0.9$ (panel (a)) and $\gamma_{[0.3]} \simeq 0.8$ (panel (b)) both extended over the whole observation-window $\tau \leq 10^7$. While the empirical ergodic threshold $\beta_* \simeq 10^{-4}$ and its characteristic RT range $10^4 < \tau < 10^6$ are found to be *independent* on the choice of recurrence-set (as they should), different decay rates imply that we are still observing the *non-asymptotic* part of the RT probability distribution. In other words, even ignoring the time-scale at which the true asymptotic regime will appear, we can already tell that it must be larger than $\tau = 10^7$. To our knowledge, no existing method (not analytic nor numerical) is capable to provide such lower-bound information in a completely general, higher-dimensional setting.

We remark that our Poincaré-time (PT) analysis is different from the one studied in [33, 35], although the two share the same philosophy. There, several *conditional measures* are constructed by selecting only those Poincaré cycles that have RT falling in some specific time-range, which is picked *empirically* from the RT statistics. Here, instead, we compute the *full* orbit density and the local-time of *all* Poincaré cycles to get, by PT, an *automatic* partition for phase-space *and* for RT distributions as well.

V. CONCLUSIONS

In this paper we investigate the dependence of Poincaré recurrence-times (RT) on the choice of recurrence-set. By deriving a general expression for the return prob-

abilities in terms of level-sets of a *time-function* (PT) that are easily visualized in phase-space, we are able to *localize* all the dynamical structures responsible for long recurrences by automatically *associating* each of them to a specific bin of the RT statistics. We exploit PT as a *detector* for extremely small phase-space structures (such as tiny stability-islands) based on their natural recurrence time-scale. As a second by-product, PT analysis also suggests a rigorous recipe to *enhance* the RT probabilities of a given set by simply *deforming* its shape.

By taking as a benchmark-model the process of weak Arnol'd diffusion in a four-dimensional Hamiltonian map, we discover a novel factor ruling the dependence of RT statistics on the choice of recurrence-set B : namely, the *volume* of its *departure-set* $D_B = \mathbf{f}(B) \setminus B$, quantifying the rate per iteration at which the dynamics of system \mathbf{f} extracts/re-injects its orbits from/into a set B . Such indicator adds useful information to the standard checks of what are the *dynamical structures* (*e.g.* un/stable periodic orbits) contained in the chosen recurrence-set. This is practically implemented through numerical experiments by *controlling* the departing volume $\mu(D_B)$, which leads to concrete examples of *enhanced* RT probabilities, and by *forcibly excluding* particular resonant structures from the recurrence-set. The conjoint analysis of such two operations turns out to be crucial in identifying a lower-bound for the *transient* time-scale of the system: indeed, depending on which structures are allowed to contribute to the RT statistics, we demonstrate the existence of extremely long power-like decays whose exponent γ_B *depends* on the choice of recurrence-set B for the *whole* observed time-window, which can thus be marked as transient.

We remark the generality of such phenomenon, which can be encountered in all systems endowed with a weak-coupling mechanism between chaotic sub-systems. We also point out that the same considerations can be applied to recurrence properties of *ensembles* of initial-conditions for many, weakly-coupled identical Hamiltonian systems.

ACKNOWLEDGMENTS

M.S. thanks CAPES (Brazil) for financial support through post-doctoral fellowship (PNPD), C.M. thanks CNPq, CAPES and FAPESC (all Brazilian agencies) for financial support.

Appendix A: Numerical histograms

When dealing with real data, we write the probability $P_B(\tau) = \sum_{t \geq \tau}^{\infty} \rho_B(t)$ to *do not return* in $t < \tau$ steps as:

$$P_B(\tau) = 1 - \sum_{t=1}^{\tau-1} \rho_B(t), \quad (\text{A1})$$

since this is a *finite* sum and the normalization condition $\sum_{t=1}^{\infty} \rho_B(t) = 1$ is ensured by the Poincaré recurrence theorem. Numerically, the exact RT distribution $\rho_B(\tau)$ is then replaced by the observed *number* of recurrences $r_B(\tau) = E \cdot \rho_B(\tau)$ over an ensemble of size E , the current *total* number of collected cycles. As $\rho_B(\tau)$ generates the integrated RT probability $P_B(\tau)$, also $r_B(\tau)$ sums up to the observed number $p_B(\tau)$ of events with $\text{RT} \geq \tau$:

$$p_B(\tau) = E - \sum_{t=1}^{\tau-1} r_B(t) \simeq E \cdot P_B(\tau), \quad (\text{A2})$$

so that both $r_B(\tau)$ and $p_B(\tau)$ are integer-valued, ranging between 0 and E . Once another Poincaré cycle is executed and a new $\text{RT} = \tau'$ is collected, we raise by 1 the total number of events $E \mapsto E' = E + 1$ and apply the following update rule for the numerical RT density r_B :

$$r_B(\tau) \mapsto r'_B(\tau) = \begin{cases} r_B(\tau) + 1 & , \text{ if } \tau = \tau' \\ r_B(\tau) & , \text{ else.} \end{cases} \quad (\text{A3})$$

This produces a frequency histograms for observable τ , the RT, and allows to generate the numeric RT statistics $p_B(\tau)/E \simeq P_B(\tau)$ at *finite* number of events E , as a post-process, by Eq. (A2), *after* the data collection is over. In the formal limit of an infinite number of events:

$$\lim_{E \rightarrow \infty} p_B(\tau)/E = P_B(\tau). \quad (\text{A4})$$

one recovers the RT probability $P_B(\tau) = \text{Prob}(\text{RT} \geq \tau)$.

Appendix B: Departures & Arrivals

All points *outside* set B belong to the difference $\Omega \setminus B$, obtained by removing from phase-space Ω all points in B . By the volume-preserving character of \mathbf{f} , it follows that phase-space is invariant, $\mathbf{f}(\Omega) = \Omega$, so that, by the general property for which: $\mathbf{f}(A \setminus B) = \mathbf{f}(A) \setminus \mathbf{f}(B)$ for any pair of sets A, B (the image of a difference is the difference of the images), we obtain that all points outside B go, in one iterate, in the set $\mathbf{f}(\Omega \setminus B) = \Omega \setminus B_1$, with $B_1 \equiv \mathbf{f}(B)$. We wish to find the expression for the *arrival-set* A_B , made of points that, in a single iteration, arrive in B from its outside; intuitively, this corresponds to the intersection between the set found above and B itself: $A_B = B \cap (\Omega \setminus B_1)$. By the general property of set-intersections: $A \cap (B \setminus C) = (A \cap B) \setminus C$ for any triple $A, B,$

C , and the trivial fact that $B \cap \Omega = B$ (since Ω contains any admissible set B), we get the desired expression:

$$A_B = B \cap (\Omega \setminus B_1) = (B \cap \Omega) \setminus B_1 = B \setminus B_1. \quad (\text{B1})$$

The basic properties of Lebesgue measure μ , for which $\mu(A \cap B) = \mu(B \cap A)$ and $\mu(A \setminus B) = \mu(A) - \mu(A \cap B)$ for any pair A, B , then allow to express the *arriving volume*:

$$\mu(A_B) = \mu(B) - \mu(B \cap B_1). \quad (\text{B2})$$

By repeating the same for the departure-set $D_B = B_1 \setminus B$ described in first paragraph of Sec. III and using again the volume-preserving property $\mu(B_1) = \mu(B)$ we obtain:

$$\mu(D_B) = \mu(B_1) - \mu(B_1 \cap B) = \mu(A_B). \quad (\text{B3})$$

Relation $\mu(D_B) = \mu(A_B)$ thus tells that the volume of points that *escape* B in one iteration *coincides* with the volume that enters in B from its outside. By the set-properties enlisted above, one can also prove that the arrival- and departure-set are *disjoint* $D_B \cap A_B = \emptyset$. By similar considerations, one can also find the sets $RES_B = B \cap B_1$, where *all* residence cycles take place, and $REC_B = \Omega \setminus (B \cup B_1)$, where all Poincaré recurrence cycles take place (respectively dark-red/dark-gray and white zones in Fig. 2). Interestingly, the four sets D_B, REC_B, A_B and RES_B are all mutually disjoint, while their union make up the *whole* phase-space Ω . They thus form a covering partition of phase-space which is *uniquely* induced by the dynamical processes of departure, recurrence, arrival and residence for the chosen recurrence-set B .

Appendix C: Poincaré-time (PT)

While counting RT's, we keep track of *where* each Poincaré cycle goes by collecting in phase-space the clock function $t_B(\mathbf{x})$, named *Poincaré-time* (PT). This clock is defined as the *elapsed-time* since last exit from B and is localized at orbit position \mathbf{x} . In practice, we partition a selected two-dimensional sub-space by a square-grid \mathcal{G} (*e.g.* in Sec. IV we take \mathcal{G} over *one* of the two coupled 2D phase-spaces). By naming $\chi_t = \chi(\mathbf{x}_t) \in \mathbb{N}^2$ the discrete (integer) coordinates of the grid-cell in which point \mathbf{x}_t falls, $n^{\mathcal{G}}(\chi)$ and $t_B^{\mathcal{G}}(\chi)$ are respectively the orbit-density and the PT function *summed* over all points falling in cell χ . At each step of a cycle, we *evolve* the orbit point $\mathbf{x}_{t-1} \mapsto \mathbf{x}_t$ and its discrete representation $\chi_{t-1} \mapsto \chi_t$ while *updating* both \mathcal{G} -summed density and PT function:

$$n^{\mathcal{G}}(\chi_t) \mapsto n^{\mathcal{G}}(\chi_t) + 1, \quad (\text{C1})$$

$$t_B^{\mathcal{G}}(\chi_t) \mapsto t_B^{\mathcal{G}}(\chi_t) + t. \quad (\text{C2})$$

By collecting ensembles of cycles, we approximate the \mathcal{G} -averaged Poincaré-time function $\langle t_B \rangle_{\mathcal{G}}(\chi)$ by the ratio:

$$\langle t_B \rangle_{\mathcal{G}}(\chi) = \frac{t_B^{\mathcal{G}}(\chi)}{n^{\mathcal{G}}(\chi)}. \quad (\text{C3})$$

For 2D systems, the \mathcal{G} -averaged PT function $\langle t_B \rangle_{\mathcal{G}}(\chi)$ above coincides with the true PT function $t_B(\mathbf{x})$, and any error in its approximation may only come by the representation of smooth boundaries by grid-cells of \mathcal{G} . Once we consider systems in N dimensions with $N > 2$, the true PT function $t_B(\mathbf{x})$ depends on all N variables, while the \mathcal{G} -average $\langle t_B \rangle_{\mathcal{G}}(\chi)$ still has two variables and corresponds to the projection of the true PT function further averaged over the $N - 2$ dimension *not included* in the observed 2D sub-space where $\langle t_B \rangle_{\mathcal{G}}(\chi)$ is defined. This means that, in 2D, we observe the PT *level-sets* $S_B^\tau = \{ \mathbf{x} \in \Omega \setminus B \text{ s.t. } t_B(\mathbf{x}) = \tau \}$ discretized over grid \mathcal{G} and thus uniform PT values, constant inside each S_B^τ , while in higher-dimensions we get continuous values caused by projecting many different level-sets on grid \mathcal{G} . To clearly understand the relationship between PT level-sets and RT statistics, we consider also the update rule, analogous to Eq. (A3), for the numeric RT statistics p_B :

$$p_B(\tau) \mapsto p'_B(\tau) = \begin{cases} p_B(\tau) + 1 & , \text{ if } \tau \leq \tau' \\ p_B(\tau) & , \text{ else.} \end{cases} \quad (\text{C4})$$

for which *all* bins from 1 to τ' in p_B are raised by 1 when an event τ' is detected. On the other hand, during a Poincaré cycle τ the PT clock function $t_B(\mathbf{x})$ takes all values from 1 to τ ; by considering *each point* of the cycle as an *event* for the numerical PT *probability density* $r_{t_B}(t)$, after a new RT event τ' is collected, we get all bins from 1 to τ' raised by 1. But this is exactly the *same* operation encoded in update rule (C4) for RT statistics:

$$r_{t_B}(t) \mapsto r'_{t_B}(t) = \begin{cases} r_{t_B}(t) + 1 & \text{if } t \leq \tau' \\ r_{t_B}(t) & \text{else.} \end{cases} \quad (\text{C5})$$

Since both histograms p_B and r_{t_B} are set to zero when the experiment starts, we conclude that $r_{t_B}(\tau) = p_B(\tau)$ for all τ , *i.e.* the PT probability density (among all steps of all cycles) coincides with the RT probability (among all cycles). Notably, Eq. (C5) corresponds to a Monte-Carlo approximation of volumes $\mu(S_B^\tau)$ of the *level-sets* S_B^τ of PT function $t_B(\mathbf{x})$ which, we can thus already deduce, are proportional to $P_B(\tau)$ up to normalizations.

Appendix D: Cumulative probability

Our numerical experiments collect branches of orbits that depart from set $D_B = B_1 \setminus B$, exit and then arrive in set $A_B = B \setminus B_1$ spending $\tau \geq 1$ iterations outside B . The RT probability $P_B(\tau) = \text{Prob}(RT \geq \tau)$ to return in any number $t \geq \tau$ of iterations coincides with the probability of *not* returning during the first $t < \tau$ steps. Interestingly, the set of points S_B^τ that after τ steps did not return to B is obtained by *iterating* the previous set $S_B^{\tau-1}$ that did not return after $\tau - 1$ steps and then *removing* all points that arrived in B . This leads to the recurrence relation:

$$S_B^\tau = \mathbf{f}(S_B^{\tau-1}) \setminus B. \quad (\text{D1})$$

Since the set of points that do not return in B after $\tau = 1$ iterations is just the departure-set $B_1 \setminus B \equiv D_B$, we set $S_B^1 = D_B$ as the initial condition for relation (D1) at $\tau = 1$. This leads to the intuitive explicit solution:

$$S_B^\tau = B_\tau \setminus \bigcup_{t=0}^{\tau-1} B_t, \quad (\text{D2})$$

which tells that the set of points S_B^τ not returning to B in the first τ steps is just the τ -th iterate of B with all the previous iterates *removed*, including set B itself. By initial assumption, the volumes of sets (D2) quantify the RT probability, so that $\mu(S_B^\tau) \propto P_B(\tau)$ for all τ ; since one must also have $P_B(1) = 1$ for normalization, the full RT probability has the unique expression:

$$P_B(\tau) = \mu(S_B^\tau) / \mu(S_B^1), \quad (\text{D3})$$

in terms of the set volumes $\mu(S_B^\tau)$. By labelling through the PT function $t_B(\mathbf{x}_t) \equiv t$ each of the iterates along each Poincaré cycle, we obtain a phase-space function $t_B(\mathbf{x})$ whose *level-sets* $S_B^\tau \equiv \{ \mathbf{x} \in \Omega \setminus B \text{ s.t. } t_B(\mathbf{x}) = \tau \}$ as in Eq. (3) coincide exactly with the sets in Eq. (D2), since one finds $t_B(\mathbf{x}) = \tau$ in all points in B_τ that *has not been already* labelled at any previous time $t = 0 \dots \tau - 1$. This proves that expression (D3) for RT statistics $P_B(\tau)$ (or, equivalently, Eq. (4)) corresponds to the ratio between the τ -th and the first PT level-set volume, as suggested by comparison of Eq.s (C4) and (C5) from Appendix C.

-
- [1] V. I. Arnold and A. Avez, *Ergodic Problems of Classical Mechanics* (Addison-Wesley, Boston, 1989).
[2] C. F. F. Karney, *Physica D* **8**, 360 (1983).
[3] J.-P. Bouchaud and A. Georges, *Phys. Rep.* **195**, 127 (1990).
[4] M. F. Shlesinger, G. M. Zaslavsky, and J. Klafter, *Nature* **363**, 31 (1993).
[5] T. H. Solomon, E. R. Weeks, and H. L. Swinney, *Phys. Rev. Lett.* **71**, 3975 (1993).
[6] R. Metzler and J. Klafter, *Phys. Rep.* **339**, 1 (2000).
[7] R. Artuso and R. Burioni, *Large deviations in physics*, edited by A. Vulpiani, F. Cecconi, M. Cencini, and D. Vergni (Springer, Berlin, 2014).
[8] G. Cristadoro and R. Ketzmerick, *Phys. Rev. Lett.* **100**, 184101 (2008).
[9] D. L. Shepelyansky, *Phys. Rev. E* **82**, 055202 (2010).
[10] H. Poincaré, *Acta Mathematica* **13**, 1 (1890), for a simple proof see V.I. Arnold, *Mathematical Methods of Classical Mechanics* (Springer-Verlag, New York, 1989).
[11] B. V. Chirikov and D. L. Shepelyansky, *Physica D* **13**, 395 (1984).
[12] L.-S. Young, *Ann. Math.* **147**, 585 (1998).
[13] L.-S. Young, *Isr. J. Math.* **110**, 153 (1999).

- [14] R. Artuso and C. Manchein, Phys. Rev. E **80**, 036210 (2009).
- [15] K. M. Frahm and D. L. Shepelyansky, Eur. Phys. J. B **86**, 322 (2013).
- [16] R. M. da Silva, C. Manchein, M. W. Beims, and E. G. Altmann, Phys. Rev. E **91**, 062907 (2015).
- [17] E. G. Altmann and H. Kantz, Europhys. Lett. **78**, 10008 (2007).
- [18] I. I. Shevchenko, Phys. Rev. E **81**, 066216 (2010).
- [19] R. M. da Silva, M. W. Beims, and C. Manchein, Phys. Rev. E **92**, 022921 (2015).
- [20] A. K. Mazur and D. L. Shepelyansky, Phys. Rev. Lett. **115**, 188104 (2015).
- [21] R. Artuso, G. Casati, and I. Guarneri, J. Stat. Phys. **83**, 145 (1996).
- [22] J. D. Meiss and E. Ott, Phys. Rev. Lett. **55**, 2741 (1985).
- [23] M. Hirata, B. Saussol, and S. Vaienti, Commun. Math. Phys. **206**, 33 (1999).
- [24] V. I. Arnold, Sov. Math.-Dokl. **5**, 581 (1964).
- [25] A. J. Lichtenberg and M. A. Leiberman, *Regular and Chaotic Dynamics* (Springer-Verlag, New York, 1992).
- [26] H. Kantz and P. Grassberger, Phys. Lett. A **123**, 437 (1987).
- [27] H. Kantz and P. Grassberger, J. Phys. A: Math. Gen. **21**, L127 (1988).
- [28] B. V. Chirikov, Phys. Rep. **52**, 263 (1979).
- [29] E. M. McMillan, *Some thoughts on stability in nonlinear periodic focusing systems*, Report Number: UCRL-17795 University of California, Radiation Laboratory, Lawrence Berkeley National Laboratory, U.S. D.o.E. (1967).
- [30] M. Richter, S. Lange, A. Bäcker, and R. Ketzmerick, Phys. Rev. E **89**, 022902 (2014).
- [31] G. M. Zaslavsky, Chaos **5**, 653 (1995).
- [32] S. Tomsovic and A. Lakshminarayan, Phys. Rev. E **76**, 036207 (2007).
- [33] C. V. Abud and R. E. de Carvalho, Phys. Rev. E **88**, 042922 (2013).
- [34] F. Ginelli, P. Poggi, A. Turchi, H. Chaté, R. Livi and A. Politi, Phys. Rev. Lett. **99**, 130601 (2007).
- [35] E. G. Altmann, **Ph.D. Thesis**, Chap. 6, Sec. 6.1.2 (2007).
- [36] All simulations and figures have been performed through the C++ template library for linear algebra **EIGEN** and the plotting program **GNU PLOT**.
- [37] We checked also many other values of K_j , including cases with $K_1 = K_2$, finding qualitatively similar results; the present choice is motivated by generality, to have one map ($K_1 = 0.65$) with stronger stickiness than the other ($K_2 = 0.60$) due to different phase-space structures.
- [38] Since any regular curve in phase-space may be thought as an infinite sequence of infinitesimal tangent vectors and, in general, we ignore how to design a recurrence-set B in order to have its boundary made by *covariant Lyapunov* vectors [34], it follows that all PT level-sets S_B^τ , for almost all sets B , *align* to the unstable manifold in the limit $\tau \rightarrow \infty$ of infinite recurrence-times.
- [39] Due to much longer time-scales, it is more difficult to detect tiny islands in strongly mixed backgrounds as in Fig. 3 (a) rather than almost-ergodic systems as in [32].
- [40] We remark that Poincaré-time (PT) functions can be constructed for any higher-dimensional time-series that admit meaningful phase-space representations in *at least* two variables; such analysis is postponed to future works.
- [41] Interestingly, the rectangular departure-sets satisfy the inequality $\mu(D_{B_{[0.3]}}) > \mu(D_{B_{[0.1]}})$, while such relation *reverses*, $\mu(D_{I_{[0.3]}^{200}}) < \mu(D_{I_{[0.1]}^{200}})$ for the associated lag-sets, (see Fig. 6 (b)); notice that this is solely due to the *shapes* of the iterates of the two specific recurrence-sets.